Supporting Information

CO_2 hydrogenation to light olefins over Fe-Co/K-Al_2O_3 catalysts prepared via microwave calcination

Nutkamaithorn Polsomboon [a], Thanapha Numpilai [b], Kulpavee Jitapunkul [a], Kajornsak Faungnawakij [c], Metta Chareonpanich [a,d], Xingda An [e,f], Le He [e,f], Günther Rupprechter [g] and Thongthai Witoon [a,d] *

[a] Center of Excellence on Advanced Adsorbents and Catalysts for Carbon Capture and Utilization, Department of Chemical Engineering, Faculty of Engineering, Kasetsart University, Bangkok 10900, Thailand

[b] Department of Environmental Science, Faculty of Science and Technology, Thammasat University, Pathumthani, 12120, Thailand

[c] National Nanotechnology Center (NANOTEC), National Science and Technology Development Agency (NSTDA), Pathum Thani, 12120 Thailand

[d] Center for Advanced Studies in Nanotechnology for Chemical, Food and Agricultural Industries, Kasetsart University, Bangkok, 10900, Thailand

[e] Institute of Functional Nano & Soft Materials (FUNSOM), Soochow University, Suzhou 215123, China

[f] Jiangsu Key Laboratory of Advanced Negative Carbon Technologies, Soochow University, Suzhou 215123, Jiangsu, P. R. China

[g] Institute of Materials Chemistry, Technische Universität Wien, Getreidemarkt 9/BC/01, Vienna 1060, Austria

*Corresponding author e-mail address: fengttwi@ku.ac.th (Thongthai Witoon)

1. Experimental

1.1. Catalyst characterization

The stability of Fe-Co/K-Al_2O_3 after calcination using traditional calcination and microwave calcination methods was investigated with thermal gravimetric analysis (TGA/DSC 3+ apparatus). The sample was performed under O_2 flow with a flow rate of 75 mL min^{-1} and heating rate 10 °C min^{-1} from 40 to 1000 °C. Textural properties including BET surface area and pore size distribution of the calcined catalysts were determined by N_2-sorption technique on a Micromeritics 3 Flex surface analyzer. Phase and crystallinity of different catalysts at after calcination and reaction states were examined with X-ray Diffraction (XRD) technique with a Bruker D8 Advance. The measurement spanned a 2θ range from 15° to 55°, employing a step increment of 0.05° and a count time of 1 second per point. Elemental composition of the catalysts was determined with X-ray Fluorescence (XRF) spectroscopy technique using a Bruker S8 TIGER apparatus. The reduction behavior of metal oxides of calcined catalysts was studied with H_2 temperature-programmed reduction (H_2-TPR) employing the Micromeritics AutoChem II 2920 apparatus. This involved heating a 0.1 g sample in a U-shaped quartz tube from ambient temperature to 150 °C at 10 °C per minute under an Ar flow of 50 mL min-1 for 30 min, followed by cooling temperature to 50 °C and then gas switching to a 10% H_2/Ar mixture. The H_2 consumption was monitored by thermal conductivity changes in the effluent stream as the temperature was increased to 1000 °C at 10 °C min^{-1}. Surface chemical analysis was conducted through X-ray Photoelectron Spectroscopy (XPS) using a PHI 5000 Versa Probe II Scanning XPS Microprobe UHV using Al Kα radiation source (1486.6 eV), and binding energies were benchmarked against the C1s line at 285 eV. Expanding on the H_2-TPR analysis, the Micromeritics AutoChem II 2920 apparatus was also employed to investigate the H_2-TPD and CO_2-TPD profiles of various catalysts. Each 0.1 g catalyst sample underwent in-situ reduction with a 10% H_2/90% Ar mixture (50 mL min^{-1}) at 400 °C for 5 hours, followed by cooling to 50 °C under an Ar flow (50 mL min^{-1}). For the H_2-TPD experiment, the catalyst encountered a 10% H_2/Ar mixture for 1 hour, while during the CO_2-TPD experiment, it interacted with a 10% CO_2/He mixture for an equivalent duration. Subsequently, the samples were flushed with Ar for a minimum of 30 minutes to eliminate physisorbed species. Upon achieving a stable baseline, the temperature was ramped up from 50 °C to 800 °C at a rate of 10 °C min^{-1}. These findings provided valuable insights into the interaction of H_2 with the catalyst

surface and the catalysts' surface basicity, which are crucial for understanding their reactivity and performance.

1.2. Catalytic performance test

CO_2 hydrogenation to light olefins was conducted in a fixed-bed stainless steel reactor. For each experiment, 0.5 g of the catalyst was mixed with 3.0 g of inert silica sand (75–150 μm) to improve heat distribution within the catalyst bed. Initially, the catalyst was reduced under a hydrogen flow of 60 mL min^{-1} at 400 °C for 5 h, followed by a controlled cooling to 300 °C. Subsequently, the reactor system was pressurized to 20 bar using a gas mixture of $CO_2/N_2/H_2$ in the ratios of 11/11/55 mL min^{-1}, respectively. Data collection occurred hourly over three hours before the reaction temperature was incrementally raised to 320 °C at a rate of 2 °C min^{-1}. This procedure was systematically repeated for subsequent reaction temperatures of 340 °C, 360 °C, and 380 °C. Effluent gases were analyzed using an Agilent 7820A gas chromatograph equipped with a thermal conductivity detector (TCD) and Hayesep Q and HP-Plot 5A columns for detecting CO, N_2, CH_4, and CO_2. Additionally, a Shimadzu 8A gas chromatograph, fitted with a Flame Ionization Detector (FID) and Porapak Q and OV-1 columns, was used for detailed profiling of C_1-C_{18} hydrocarbons. Quantitative assessments including CO_2 conversion, hydrocarbon and CO selectivities, hydrocarbon distribution, ratios of C_2–C_4 olefins to C_2–C_4 paraffins, and yields of C_2–C_4 olefins were conducted. Nitrogen was used as an internal standard. Calculations were based on designated equations (Eq. (1) to Eq. (7)).

$$CO_2 \text{ conversion } (\%) = \left(\frac{\frac{\text{moles } CO_{2in}}{\text{moles } N_{2in}} - \frac{\text{moles } CO_{2out}}{\text{moles } N_{2out}}}{\frac{\text{moles } CO_{2in}}{\text{moles } N_{2in}}} \right) \times 100 \quad (1)$$

$$\text{Selectivity to hydrocarbon}_i \ (\%) = \frac{i \bullet \left(\frac{\text{moles hydrocarbon}_{i,out}}{\text{moles } N_{2out}} \right)}{\left(\frac{\text{moles } CO_{2in}}{\text{moles } N_{2in}} - \frac{\text{moles } CO_{2out}}{\text{moles } N_{2out}} \right)} \times 100 \quad (2)$$

i = atomic number of carbon

$$\text{Selectivity to CO (\%)} = \frac{\left(\frac{\text{moles CO}_{\text{out}}}{\text{moles N}_{2\text{out}}}\right)}{\left(\frac{\text{moles CO}_{2\text{in}}}{\text{moles N}_{2\text{in}}} - \frac{\text{moles CO}_{2\text{out}}}{\text{moles N}_{2\text{out}}}\right)} \times 100 \quad (3)$$

$$\text{Hydrocarbon distribution}_{\text{i}}\ (\%) = \frac{i \times \text{moles hydrocarbon}_{\text{i}} \times 100}{\sum_{i=1}^{n} i \times \text{moles hydrocarbon}_{\text{i}}} \quad (4)$$

$$\text{Olefins to paraffins ratio } (C_2 - C_4) = \frac{2 \text{ x moles of } C_2H_4 + 3 \text{ x moles of } C_3H_6 + 4 \text{ x moles of } C_4H_8}{2 \text{ x moles of } C_2H_6 + 3 \text{ x moles of } C_3H_8 + 4 \text{ x moles of } C_4H_{10}} \quad (5)$$

$$\text{Light olefin yields } (C_2 - C_4) = \left(\frac{CO_2 \text{ conversion}}{100}\right) \times \left(\frac{\text{Selectivity of } C_2 - C_4 \text{ olefins}}{100}\right) \quad (6)$$

$$\text{Carbon balance (\%)} = \left(\frac{\text{Total moles of carbon in products}}{\text{Total moles of } CO_2 \text{ converted}}\right) \times 100 \quad (7)$$

The carbon balances were maintained within a tight range of 95% to 99%, indicating a high degree of reaction efficiency and data reliability.

2. Results and discussion

Table S1 BET surface area, BJH mean pore size and pore volume measured by N_2-sorption technique of Fe-Co/K-Al_2O_3 catalysts prepared via traditional calcination (C) and microwave calcination at different powers (H, MH, M and ML).

Catalysts	BET surface area (m^2 g^{-1})	BJH mean pore size (nm)	Pore volume (cm^3 g^{-1})	Elements (wt%)			
				Fe	Co	K	Al
C	44.2	26.9	0.22	32.9	7.4	14.6	26.4
H	41.4	28.4	0.25	31.6	7.0	14.2	27.0
MH	42.4	25.1	0.24	32.4	7.1	14.3	26.8
M	42.3	24.2	0.25	31.8	7.2	14.4	26.9
ML	40	24.2	0.23	32.6	7.3	14.5	26.6

Hydrogen adsorption characteristics across various catalysts were analyzed using the H_2-TPD technique, with findings illustrated in Figure S2a. The H_2-TPD profile for the catalyst prepared by traditional calcination (C) identifies four distinct desorption peaks—δ, α, β, and γ. These peaks represent physically adsorbed H_2, chemisorbed hydrogen over metallic Fe sites, hydrogen interactions at the interface between metallic species and unreduced metal oxides (e.g., $KFeO_2$ and $KAlO_2$), and strongly adsorbed hydrogen on $KAlO_2$ due to spillover from Fe species, respectively [1–3].

The application of microwave calcination resulted in an increased α peak and a decreased β peak, indicating a higher presence of isolated Fe particles in the microwave-calcined catalysts (H, MH, M, ML). The distribution of hydrogen adsorption across these interactions and the corresponding fractions (%) are detailed in Table S2. For example, with catalyst C, adsorption capacities for peaks δ, α, β, and γ were measured at 7.0, 7.0, 122.1, and 141 μmol g^{-1}, constituting 2.5%, 2.5%, 44.1%, and 50.9% of the total adsorption, respectively. At the highest microwave power of 700 W (H), these capacities changed to 11.9, 34.6, 135.4, and 173.1 μmol g^{-1}, accounting for 3.4%, 9.7%, 38.1%, and 48.8% of the total, respectively. Reducing microwave power from H to MH, M, and ML correlated with increased α peak fractions and decreased β peak fractions, suggesting a rise in isolated Fe particles with weaker hydrogen interactions. These H_2-TPD

findings are supported by trends in Fe-M species and Fe-C/Fe_3O_4 ratios, as analyzed by XPS (Tables 2 and 3).

The CO_2-TPD profile of the C catalyst, shown in Figure S2b, reveals four desorption peaks at temperatures of 100 °C (δ), 180 °C (α), 310 °C (β), and 498 °C (γ). The corresponding CO_2 adsorption amounts are 23.9, 55.6, 157.9, and 86.1 μmol g^{-1}, respectively (Table S3). These peaks indicate varying strengths of CO_2 interaction with the catalyst surface, from weakest (δ) to strongest (γ). Under microwave calcination at different power levels, the α peak's adsorption capacity consistently exceeded that of the C catalyst, showing figures of 84.5, 74.4, 68.4, and 60.1 μmol g^{-1}. Conversely, the γ peak's strong basicity decreased from 86.1 μmol g^{-1} in the C catalyst to lower values in microwave-calcined samples, suggesting a shift towards weaker basic sites under microwave treatment.

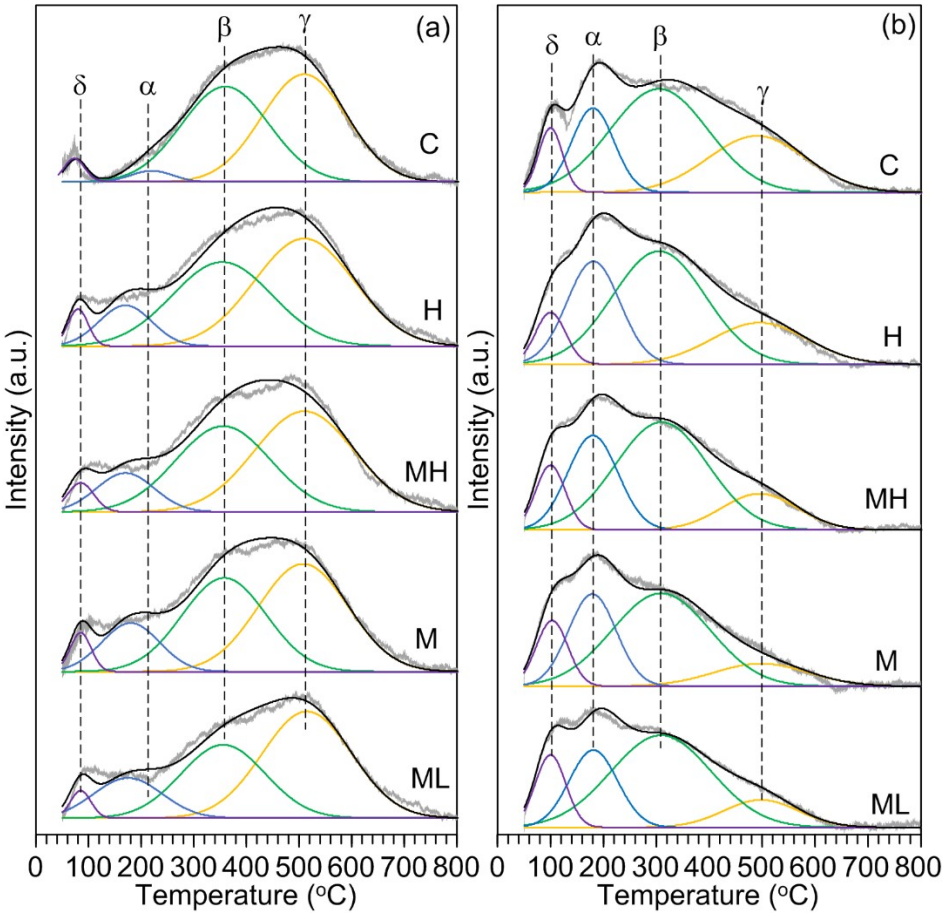

Figure S2 H_2-TPD (a) and CO_2-TPD (b) profiles of pre-reduced FeCoKAl catalysts. Both sets of profiles compare catalysts prepared using traditional calcination (C) and microwave-assisted calcination at varying power levels: 700 W (H), 616 W (MH), 511 W (M), and 364 W (ML).

Table S2 H_2 adsorption on pre-reduced FeCoKAl catalysts.

Catalysts	Amount of H_2 desorbed at different sites (μmol g^{-1}) and corresponding fraction (%)			
	δ	α	β	γ
C	7.0 (2.5 %)	7.0 (2.5 %)	122.1 (44.1 %)	141 (50.9 %)
H	11.9 (3.4 %)	34.6 (9.7 %)	135.4 (38.1 %)	173.1 (48.8 %)
MH	12.3 (3.6 %)	36.2 (10.6 %)	130.7 (38.3 %)	162.0 (47.5 %)
M	13.2 (3.9 %)	45.0 (13.2 %)	127.0 (37.3 %)	155.2 (45.6 %)
ML	9.9 (3.2 %)	44.0 (14.4 %)	99.0 (32.4 %)	153.0 (50 %)

Table S3 CO_2 adsorption on pre-reduced FeCoKAl catalysts.

Catalysts	Amount of CO_2 desorbed at different sites (μmol g^{-1}) and corresponding fraction (%)			
	δ	α	β	γ
C	23.9 (7.4 %)	55.6 (17.2 %)	157.9 (48.8 %)	86.1 (26.6 %)
H	24.0 (7.2 %)	84.5 (25.3 %)	163.4 (49.0 %)	61.7 (18.5 %)
MH	30.1 (9.9 %)	74.4 (24.5 %)	156.1 (51.4 %)	43.3 (14.3 %)
M	32.3 (11.7 %)	68.4 (24.7 %)	142.2 (51.4 %)	33.7 (12.2 %)
ML	34.2 (12.7 %)	60.1 (22.4 %)	142.3 (53.0 %)	32.1 (11.9 %)

Energy consumption for both conventional and microwave calcination methods was directly calculated from the electrical current supplied to each device. For conventional calcination in a muffle furnace, the temperature was escalated to 400 °C at a rate of 2 °C per minute and sustained at that level for 4 h before allowing natural cooling to ambient temperature. The current, varying with temperature due to changes in heater resistance, was monitored and recorded (Figure S3). These current measurements were used to calculate energy consumption with the following equation:

$$E_C = \left(\int_0^{t_1} I_H(t)\mathrm{d}t + \int_{t_1}^{t_2} I_h(t)\mathrm{d}t \right) V \times 1000 \qquad \text{(Eq. 3)}$$

where I_H and I_h are the currents during heating and holding phases, respectively, and V is the voltage (230 V). The total energy consumption for the conventional calcination process, as

detailed in Table S4, is calculated to be 11.06 kWh. This total comprises 5.16 kWh consumed during the heating stage and 5.90 kWh during the holding stage.

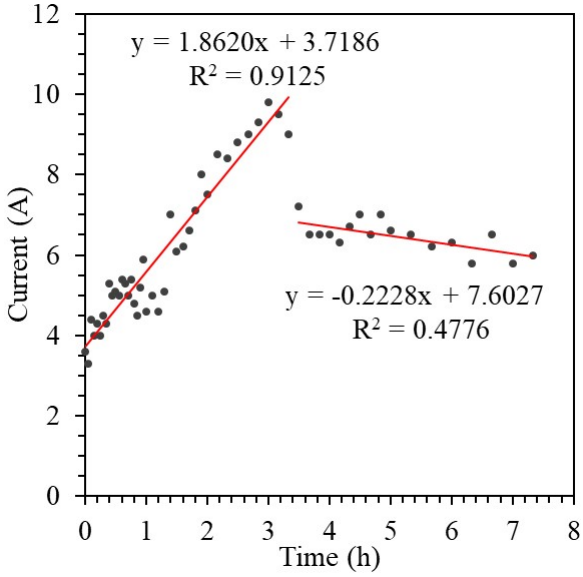

Figure S3 The measured electrical current over time during the conventional calcination process in a muffle furnace.

Table S4 Energy consumption calculation for conventional calcination by muffle furnace.

Stage	Initial time (h)	final time (h)	I (t)	Energy consumption (kW·h)
Heating	0	3.333	1.8620t+3.7186	5.16
Holding	3.333	7.333	-0.2228t+7.6027	5.90
			Summation	11.06

Microwave calcination employed a domestic microwave oven with samples irradiated for 4 min across different power settings (700 W, 616 W, 511 W, 364 W). Each power setting cycled between an irradiation stage and a rest stage every 30 seconds. The current during these stages was consistent, recorded at 5.2 A for irradiation and 0.2 A for the rest stage. The energy consumption was calculated using:

$$E_{Mw} = \frac{t_i I_i + t_r I_r}{30} V t_o \times 1000 \qquad \text{(Eq. 4)}$$

where t_i and t_r are the duration times of the irradiation and rest stages. I_i and I_r are the currents, V is the voltage (230 V) and t_o is total operating time. As indicated in Table S5, the total energy consumption for catalysts calcined using the microwave technique ranged from 0.044 to 0.080 kWh, representing a reduction of more than 99% compared to the 11.06 kWh consumed by conventional calcination in a muffle furnace.

Table S5 Energy consumption calculation for microwave calcination by domestic microwave oven at different power settings.

Power setting	Stage	Duration (s)	Average input power (kW)	Energy consumption (kWh)
700 W (H)	Irradiation	30	1.196	0.080
	Rest	0	0	
616 W (MH)	Irradiation	26	1.0365	0.070
	Rest	4	0.0061	
511 W (M)	Irradiation	22	0.8771	0.059
	Rest	8	0.0122	
364 W (ML)	Irradiation	16	0.6379	0.044
	Rest	14	0.0215	

Table S6 Catalytic performance comparison of various catalysts for CO_2 Hydrogenation to light olefins.

Catalysts	T (ºC)	P (MPa)	WHSV (mL g_{cat}^{-1} h^{-1})	CO_2 Conversion (%)	CO Selectivity (%)	Hydrocarbon distribution (%)				$C_{2=} - C_{4=}$ yield (%)	O/P	Reference
						CH_4	$C_{2-} - C_{4-}$	$C_{2=} - C_{4=}$	C_{5+}			
0.5K- Fe-Co/Al_2O_3	340	2	9000	41.2	10.6	26.8	10.2	44.4	18.6	16.4	4.4	[3]
$KFeMnMg_{0.15}$	320	3	4000	25.2	19.6	25.2	13.6	61.2	n/a	15.4	4.48	[4]
Na-$CoFe_2O_4$/CNT	340	1	3600	34.4	18.6	14.8	5.5	38.8	40.9	10.9	7.05	[5]
10Mn-Fe_3O_4	350	2	4000	44.7	9.4	22.0	7.1	46.2	24.7	18.7	6.5	[6]
Fe-Co/K-Al_2O_3	340	2	9000	40.0	12.2	24.8	7.9	46.1	21.2	16.2	5.9	[7]
0.8Fe@N-OMC	320	3	4800	53.6	4.6	12.8	46.1	40.8	0.3	20.9	0.89	[8]
Na-$CoFe_2O_4$	320	3	7200	41.8	9.7	22.1	7.6	41.2	29.0	15.5	5.39	[9]
K-CoO_x/H-ZSM-5	300	2.2	36000	22.4	17.8	46.3	7.8	33.0	12.9	6.1	4.25	[10]
0.3-CoFe/0.7-ZrO_2	320	2	4800	48.0	9.0	18.0	16.0	38.0	28	16.6	2.38	[11]
Fe-Co-DMC	320	2	3600	39.1	13.0	36.0	8.1	44.3	11.6	15.1	5.47	[12]
K/$LaFeZnO_3$	320	2	1000	48.5	25.7	15.6	16.9	41.0	26.5	14.8	2.43	[13]
NaFe	320	3	n/a	33.7	17.2	17.7	55.6	47.1	26.7	13.1	0.85	[14]
Fe	320	1.5	3000	26.3	33.8	22.5	5.7	51.4	20.4	8.9	8.95	[15]
Fe-Zn	320	0.5	3000	26.3	34.9	26.9	5.2	49.2	18.7	8.4	9.41	[15]
Fe-Co-Ni-MOFs	320	1	11040	47.5	7.3	18.4	25.4	50.4	5.8	22.2	1.99	[16]
Fe_2O_3@ZrO_2	340	3	10000	35.4	19.8	19.0	16.7	44.4	19.9	12.6	2.66	[17]
Fe-Co/K-Al_2O_3 (MH)	360	2	9240	59.3	11.7	34.1	7.3	46.8	11.8	**24.5**	6.41	This work
Fe-Co/K-Al_2O_3 (C)	360	2	9240	54.0	16.0	31.6	7.4	48.5	12.5	**22.0**	6.55	This work

References

[1] R. Satthawong, N. Koizumi, C. Song, P. Prasassarakich, *Catal. Today,* 2015, **251**, 34–40.

[2] F. Bozso, G. Ertl, M. Grunze, M. Weiss, *Appl. Surf. Sci.,* 1977, **1**, 103–119.

[3] T. Numpilai, N. Chanlek, Y. Poo-arporn, C.K. Cheng, N. Siri-Nguan, T. Sornchamni, M. Chareonpanich, P. Kongkachuichay, N. Yigit, G. Rupprechter, J. Limtrakul, T. Witoon, *ChemCatChem,* 2020, **12**, 3306–3320.

[4] K. Liu, D. Xu, H. Fan, G. Hou, Y. Li, S. Huang, M. Ding, *ACS Sustainable Chem. Eng*., 2024, **12**, 2070–2079.

[5] K.Y. Kim, H. Lee, W.Y. Noh, J. Shin, S.J. Han, S.K. Kim, K. An, J.S. Lee, *ACS Catal*., 2020, **10**, 8660–8671.

[6] J. Jiang, C. Wen, Z. Tian, Y. Wang, Y. Zhai, L. Chen, Y. Li, Q. Liu, C. Wang, L. Ma, *Ind. Eng. Chem. Res*., 2020, **59**, 5, 2155–2162.

[7] N. Chaipraditgul, T. Numpilai, C. Kui Cheng, N. Siri-Nguan, T. Sornchamni, C. Wattanakit, J. Limtrakul, T. Witoon, *Fuel,* 2021, **283**, 119248.

[8] P. Zhang, F. Han, J. Yan, X. Qiao, Q. Guan, W. Li, *Appl. Catal. B-Environ.,* 2021, **299**, 120639.

[9] F. Yuan, G. Zhang, J. Zhu, F. Ding, A. Zhang, C. Song, X. Guo, *Catal. Today,* 2021, **371**, 142-149.

[10] R. Liu, D. Leshchev, E. Stavitski, M. Juneau, J.N. Agwara, M.D. Porosoff, *Appl. Catal. B-Environ.,* 2021, **284**, 119787.

[11] Q. Zhao, X. Xu, G. Fan, F. Li, *Ind. Eng. Chem. Res.,* 2023, **62**, 9420-9432.

[12] G. Singh, S. Panda, J. Gahtori, P. Rajendra Chandewar, P. Kumar, I.K. Ghosh, A. Biradar, D. Shee, A. Bordoloi, *ACS Sustainable Chem. Eng.,* 2023, **11**, 11181–11198.

[13] L.-h. Ma, X.-h. Gao, J.-l Zhang, J.-j. Ma, X.-d. Hu, Q.-j Guo, *J. Fuel Chem. Technol*., 2023, **51**, 101–110.

[14] H. Qi, W. Si, Z. Xu, G. Wang, X. Liu, C. Lyu, B. Huang, N. Tsubaki, C. Xing, J. Sun, *ChemSusChem,* 2024, **17**, e202400484.

[15] X. Liu, M. Xu, C. Cao, Z. Yang, J. Xu, *Chin. J. Chem. Eng.,* 2023, **54**, 206–214.

[16] Y. Zhao, J. Ma, J. Yin, H. Han, X. Zhang, Y. Cao, W. Cai, *Appl. Surf. Sci.,* 2024, **657**, 159783.

[17] F. Xu, X. Meng, R. Zhao, D. Jin, W. Dai, D. Yang, Z. Xin, *Chem. Eng. J.,* 2024, **494**, 152926.